

Mesoscopic Simulation of Heat Transfer and Fluid Flow in Laser Powder Bed Additive Manufacturing

Y.S. Lee and W. Zhang

* Welding Engineering Program, Department of Materials Science and Engineering,
The Ohio State University, Columbus, OH 43221

REVIEWED

Abstract

Laser-powder bed fusion (L-PBF) additive manufacturing involves complex physics such as heat transfer and molten metal flow, which have a significant influence on the final build quality. In this study, transport phenomena based modeling is used to provide a quantitative understanding of complex molten pool transients. In particular, a three dimensional (3D), transient numerical model is developed for L-PBF additive manufacturing by solving the governing partial differential equations of mass, momentum and energy conservation. The individual powder particles are resolved using the volume of fluid method (VOF) method with a fine mesh size of 3 μm (thus at meso-scale). The powder particle arrangement including particle size distribution and packing density are taken into account in placement of individual particles calculated using discrete element method. Moreover, the model considers Marangoni shear stress, an important driving force for molten metal flow. The numerical model is used to quantitatively study the effect of laser power, scanning speed, and powder size distribution on the bead geometry and formation of balling defect.

Keywords: Particle size distribution, additive manufacturing, volume of fluid, powder bed fusion

1. Introduction

Laser-powder bed fusion (L-PBF) additive manufacturing involves complex physical processes such as beam absorptance, heat transfer and molten metal flow, phase transformation, and thermal stress and distortion; all these factors influence the final build quality and properties [1,2]. Absorbed beam energy in the powder bed melts the particles and causes strong fluid flow in the molten pool which is driven by surface tension gradient (or Marangoni shear stress). Because of the highly dynamic fluid flow, the shape of the molten pool surface, which is a free surface, is constantly evolving. The above physics is similar to that in laser beam welding. However, the powder particles in L-PBF (as opposed to a solid metal in laser welding) add significant complexity to the process. In particular, the absorptance of laser beam depends on particle size distribution and particle arrangement (or stack-up). The weld pool shape as well as the heat transfer and fluid flow are also significantly affected by local arrangement of powder particles in the powder bed which can vary from location to location due to randomness of the particles size and distribution. In other words, the heat dissipation can become anisotropic, which in turn, can alter local temperature gradient and fluid flow field.

Give the extremely wide length scale of L-PBF physics, numerical models of L-PBF process can be approximately divided into two groups. The first group deals with phenomena at

the engineering scale (e.g., mesh size on the order of 1 mm). For instance, finite element method (FEM) based models are employed to describe the evolution of temperature, stress and displacement fields during L-PBF [3,4]. Obviously, given the coarse mesh resolution, melting of powder particles in individual tracks are not simulated in the FEM based models, although those models can easily study the global variation of temperature, residual stress and distortion in the entire part. The second group comprises meso-scale models capable of resolving individual powder particles (e.g., mesh size on the order of 1 μm). An example of such meso-scale models is the two dimensional (2D) heat transfer and fluid flow model based on lattice Boltzmann method (LBM) developed by Korner et al. for single layer [5] and multiple layers [1]. The free surface was tracked using the volume of fluid method (VOF). The 2-D model was used to create a process map which showed that the molten pool characteristics were considerably affected by laser scanning speed, beam power and powder packing density. Three dimensional (3D) model based on LBM was developed by Khairallah and Anderson [6] and by Gurtler et al. [7]. Consideration of particle size distribution and stack-up varied from model to model from simple mono-size [7] to random size distribution [5]. It is noted that LBM is a newer method than the conventional finite difference/volume method to solve the governing transport equations. Even at a mesh (cell) size of 3 μm , the LBM is computationally demanding, which can easily consume on the order of 10,000 CPU hours. Moreover, it can be difficult to consider some important temperature dependent material properties such as surface tension gradient and viscosity which can influence heat transfer and fluid flow behavior.

The present paper uses two models in sequence. The first model is a powder particle packing model based on discrete element method (DEM). It provides the particle stack-up information (e.g., locations and radii of individual particles). Such information is then input into the second model, which is a high resolution but computationally less demanding, heat transfer and fluid flow model based on the finite difference method and VOF. This 3D transient model is applied to understand the correlation of powder packing characteristics, process parameters, and molten pool dynamics to the resultant surface quality (e.g., balling defect).

2. Numerical modeling approach

2.1. Discrete element method simulation of powder packing

DEM is a well-established numerical method that is capable of simulating the motion of a large number of individual particles including contact interactions between particles/particles and particles/walls. In the present study, a powder packing model is developed based on Yade, an open source software package for DEM. For brevity, only salient features of the DEM model are described below and the details are available in Yade documentation [8].

The powder particles are simplified as elastic spheres with different radii and the powder container is treated as rigid walls. Each particle has six velocity components: three translational and three rotational in the x, y and z axis of a Cartesian coordinate system. To efficiently track the large number of contact interactions, a Hertz based soft-contact formula is used which permits a finite overclosure locally at the contact point between particles. The normal contact force is then calculated using the Hertz solution of force versus overclosure. The tangential forces are calculated using the Coulomb friction law. These contact forces are summed together with the gravitational force to obtain the total forces and moments exerting on a particle. The solution process in DEM is the following. At each time step, the total forces and moments for individual particles are

calculated based on the procedure above. Next, the velocities are calculated by solving Newton's second law of motion. Finally, the particle positions are updated with distances traveled (i.e., multiplication of velocities and time step size) and the calculation continues to the next time step.

To study the effect of particle size on the molten pool dynamics, two particle size distributions (PSDs) are considered, as shown in Fig. 1. Both PSDs have the same range of particle radii from 10 μm (minimum) to 20 μm (maximum). Fig. 1(a) and 1(b) show a positively skewed PSD (abbreviated as PSD+) with a mean radius of 12.7 μm and a negatively skewed PSD (abbreviated as PSD-) with a mean radius of 17.3 μm , respectively. As shown in Fig. 1(c), PSD+ contains a higher fraction of small particles. For example, 90% of the particles in PSD+ have a radius less than 14 μm , while that fraction is only 8% in PSD-.

The spherical particles considered in the present DEM simulation are made of INCONEL® Alloy 718 (IN718), a nickel alloy with good high-temperature strength. The key material properties for DEM include Young's modulus = 195 GPa, and friction coefficient between particles = 0.3. In the DEM simulation, a cloud of particles with the given PSD is first generated inside a rectangular box without any overclosure among particles. The particles then fall down onto the floor of the containing box by gravity and eventually settled down. In the DEM, the packed particles are then subject to a roller with a clearance of 50 μm to create a nominally 50- μm -thick layer. The positions (i.e., x, y and z coordinates) and radii of the stabilized particle are then exported and used to define the initial geometry in the subsequent heat transfer and fluid flow model described in the following section.

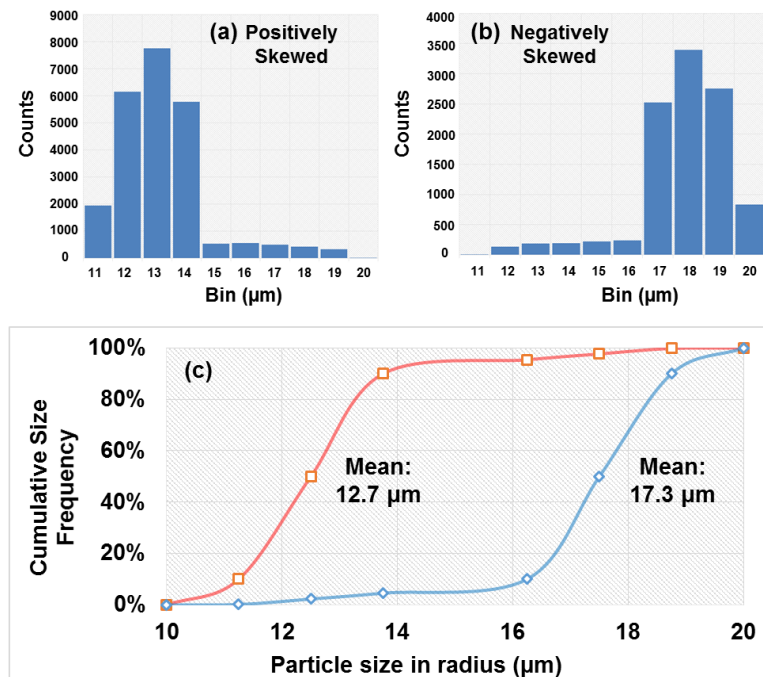


Figure 1: Histograms of (a) positively skewed PSD, (b) negatively skewed PSD, and (c) cumulative size frequency for the two PSDs in (a) and (b).

2.2 Governing equations for heat transfer and fluid flow

The L-PBF process simulation is performed based on numerical solution of mass, energy and momentum conservation equations, which are given in Eqns. (1) through (3), respectively.

$$\text{Mass:} \quad \nabla \cdot \vec{v} = 0. \quad (1)$$

$$\text{Energy:} \quad \frac{\partial h}{\partial t} + (\vec{v} \cdot \nabla)h = \frac{1}{\rho} (\nabla \cdot \lambda \nabla T). \quad (2)$$

$$\text{Momentum:} \quad \frac{\partial \vec{v}}{\partial t} + (\vec{v} \cdot \nabla)\vec{v} = -\frac{1}{\rho} \nabla P + \mu \nabla^2 \vec{v} + \vec{g}[1 - \beta(T - T_m)]. \quad (3)$$

where \vec{v} is molten metal velocity, h is enthalpy, t is time, ρ is fluid density, T is temperature, λ is thermal conductivity, P is hydrodynamic pressure, μ is viscosity, g is gravitational acceleration in z direction, β is coefficient of thermal expansion, and T_m is melting temperature of material. In Eqns. (1) and (3), the fluid is assumed to be incompressible and Newtonian with laminar flow.

The position of molten pool surface is not known *a priori*. The VOF method is used to track the position and shape of the molten pool surface (free surface). It solves a scalar transportation equation for the volume fraction of fluid in a cell (F) as:

$$\text{VOF:} \quad \frac{\partial F}{\partial t} + \nabla \cdot (\vec{v}F) = 0. \quad (4)$$

A cell is void when $F = 0$, and completely occupied by the fluid when $F = 1$. When the value of F is between 0 and 1, an interface between the fluid and void exists in the cell.

The conversation equations (1) through (4) are discretized and then solved using the finite difference method in Flow-3D, a commercial computational fluid dynamics (CFD) code. Details of the discretization and solution steps are available in the literature [9,10].

2.3 Computational domain, boundary conditions and materials properties

The transient simulation is performed in a 3D computation domain with 1000 μm (length), 270 μm (width) and 190 μm (height), as shown in Fig. 2. The domain comprises a 50- μm -thick layer of powder particles laying on a 90- μm -thick substrate. The remainder of the domain is initially filled with void. The powder layer geometry is initialized using the results from the previous DEM simulation. To maximize spatial resolution while reducing the total number of cells, biased meshing is utilized where the mesh size reduces continuously from 9 μm to 3 μm in the substrate toward the substrate/powder layer interface. The mesh size is kept constant 3 μm in the powder layer and the void above it. The total number of cells is 1.43 million.

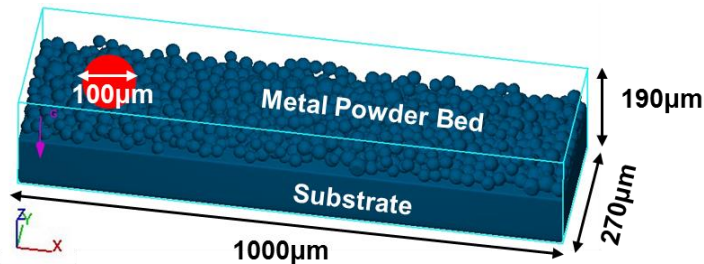


Figure 2: Schematic description of computational domain.

The primary boundary condition for solving the energy conservation equation is the heat input from the scanning laser beam. The absorption of laser energy by the powder particles is complex. To make the simulation tractable, a prescribed heat flux boundary condition based on Gaussian distribution is imposed on the top surface of the powder layer [11]. For the molten metal fluid flow, the temperature dependent surface tension and the resultant Marangoni shear stress are important driving forces for both the molten metal convection and the evolution of free surface shape. In the present study, the temperature dependency of surface tension is included with an improved surface tension model available in Flow-3D [9].

The temperature dependent thermo-physical properties of IN718 including density, thermal conductivity, specific heat and liquid metal viscosity are plotted in Fig. 3 [9]. Additional thermo-physical properties and L-PBF processing parameters are summarized in Table 1 [9].

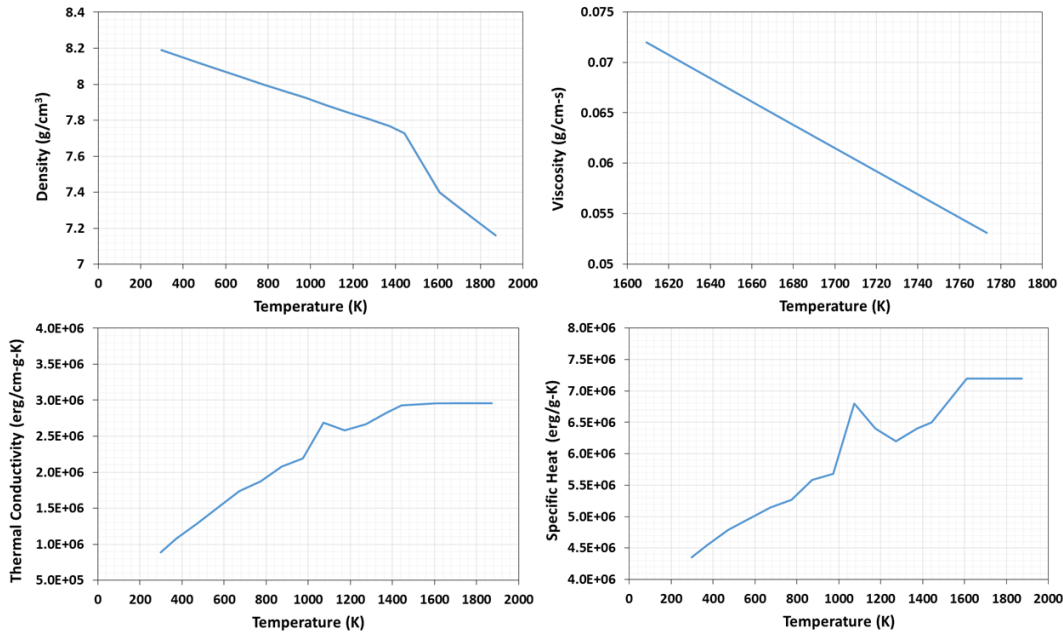


Figure 3: Thermo-physical properties of IN718. Note 1 erg = 10⁻⁷ joules.

Table 1: Additional thermo-physical properties of IN718 and L-PBF processing parameters.

Property and Parameters	Value [units]
Liquidus	1608.15 [K]
Solidus	1523.15 [K]
Surface Tension	1882 [g/s ²]
Temperature Coefficient of Surface Tension	-0.1 [g/s ² K]
Laser Beam Spot Size	100 [μm]
Laser Power	150 and 200 [W]
Scanning Speed	1.1 and 2.3 [m/s]
Powder Packing Density	38 and 45 [%]

As described previously, even for the fairly small computational domain shown in Fig. 2, there are more than 1 million cells in order to accurately resolve the individual particles. At this level of resolution, the transient simulation of about 600-microseconds-long L-PBF takes approximately 40 hours clock time to finish in a moderately powerful workstation with Intel® Xeon® Processor E5335 and 4 GB RAM. Compared with thousands of CPU hours needed by LBM, the present model based on finite difference method and VOF, incorporating temperature-dependent surface tension, is more computationally efficient. Obviously, the current domain is limited to simulating a single linear track of laser melting. To consider more complex laser scanning patterns and multilayers, the present model will need to be scaled up by utilizing distributed memory parallel computing in the future. Nevertheless, the present model allows the study of the correlation of powder packing characteristics, process parameters, and molten pool dynamics to the resultant surface quality, as discussed in the following.

3. Result and discussion

3.1 Stack-up of powder particles with different PSDs

Fig. 4 plots a 3D view of the stack-up of powder particles calculated using the DEM model for those two different PSDs in Fig. 1. The spherical particles are colored based on their respective radii. As shown in Fig. 4(a), the 50- μm -thick region filled with particles of PSD+ is made up with two layers of small particles at the majority of locations. This is due to the large fraction of smaller particles in PSD+. On the other hand, the region filled with particles of PSD- is mostly made up with a single layer of larger particles, as shown in Fig. 4(b). The packing density, defined as the ratio of the occupied volume by the particles to the total volume enclosing all the particles, is about 38% for both PSDs.

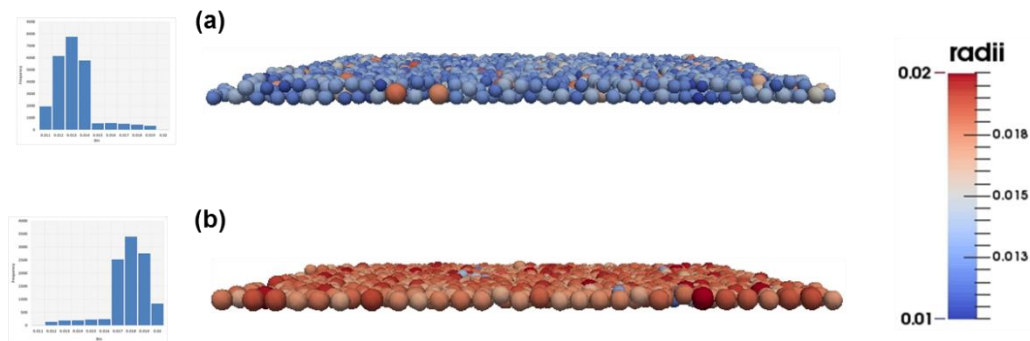


Figure 4: Stack-up of spherical particles with different particle size distributions calculated using DEM: (a) PSD+ containing a high fraction of smaller particles, and (b) PSD- containing larger particles. The radii are given in mm.

3.2. Fluid flow and molten pool shape

Fig. 5 plots the longitudinal section view (i.e., a section parallel to the laser travel direction) of temperature and velocity fields in the molten pool at time=55 μs . The temperatures are plotted as color contours and the velocities as arrows. The magnitude of the velocity is represented by the length of an arrow. The molten pool boundary is represented by the isotherm at 1608.15 K, which

is the liquidus temperature of IN718. As shown to the right side of Fig. 5, a particle is partially melted into the molten pool. Near the molten pool surface, the molten metal is pulled from the center location directly underneath the laser beam to the rear end of the pool. Such flow pattern is driven by the temperature-dependent surface tension. In other words, the center directly underneath the laser is heated to a higher temperature than the rear end. As a result, the surface tension is lower in the center than the rear end, which drives the molten metal flowing backward near the surface. Such backward flow is strong, resulting in an anticlockwise pattern as the molten metal returns from the rear end to the center inside the pool. Moreover, some of the molten metal pushed to the back flows radially and returns back to the front.

The backward flow of molten metal near the pool surface produces a surface profile that is depressed underneath the laser beam while it forms a hump toward the rear end of the pool. As discussed in the following section, the humped shape can lead to the formation of balling.

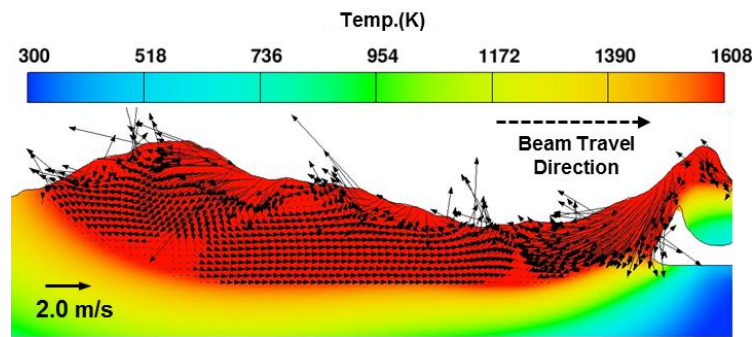


Figure 5: Longitudinal section view of heat transfer and fluid flow in the molten pool. The parameters are scanning speed = 1.1m/s, laser power = 150W, packing density = 45%, and PSD+.

3.3. Formation of balling defect

Balling is a defect that can occur when the molten pool becomes discontinuous and breaks into separated islands. Using the heat transfer and fluid flow model, it is quantitatively studied the effect of various parameters, which include PSD, scanning speed, laser beam power and powder packing density, on the formation of balling defect in L-PBF. The results are described as follows.

3.3.1. Effect of particle size distribution

A 3D view of the molten pool temperature field for the two different PSDs is shown in Fig. 6. For clarify, the fluid velocities are not plotted. For either PSD, the molten pool is continuous and the balling defect does not occur. On the other hand, the molten pool shape appears smoother for the case with PSD+ in Fig. 6(a) than that with PSD- in Fig. 6(b). As discussed previously, PSD+ contains a large fraction of smaller particles. For the same laser energy, smaller particles are more likely to be melted completely due to their smaller volume/mass, whereas larger particles are more likely to be partially melted. As a result, the molten pool formed by partially melted, large particles creates a more corrugated edge. This observed effect of PSD from the simulation results is consistent with the literature data that smaller particles can help reduce the surface roughness [12,13].

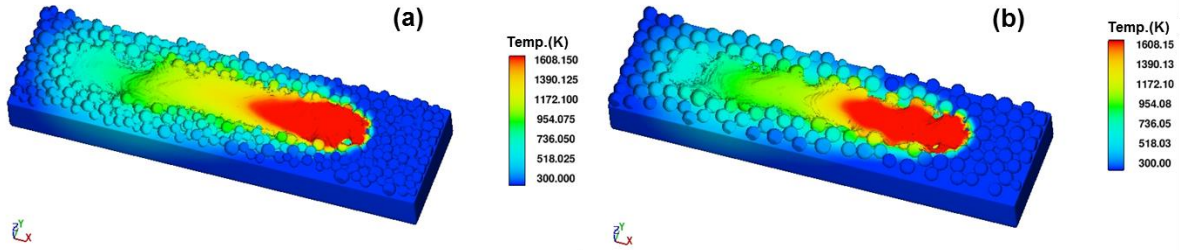


Figure 6: Calculated temperature fields showing the molten pool profile for (a) PSD+ and (b) PSD-. The parameters are scanning speed = 1.1 m/s, laser power = 200W, and powder packing density = 38%.

3.3.2. Effect of scanning speed

A faster scanning speed without defects is always desirable for higher productivity. However, if the scanning speed is too high, the molten pool may become so elongated that it can break into separate islands. Such formation of balling defect is illustrated in Fig. 7, for which the processing conditions are the same as those for Fig. 6(a) except that the scanning speed is increased to 2.3 m/s from 1.1 m/s. As shown in this figure, there is a very shallow melting of the substrate due to the high scanning speed and the resultant low heat input per unit length. Small disconnected islands (or balls) are formed in the trailing end of the molten pool. Such separate islands at the fast scanning speed are in contrast to the continuous, smooth molten pool at the slow scanning speed shown in Fig. 6(a).

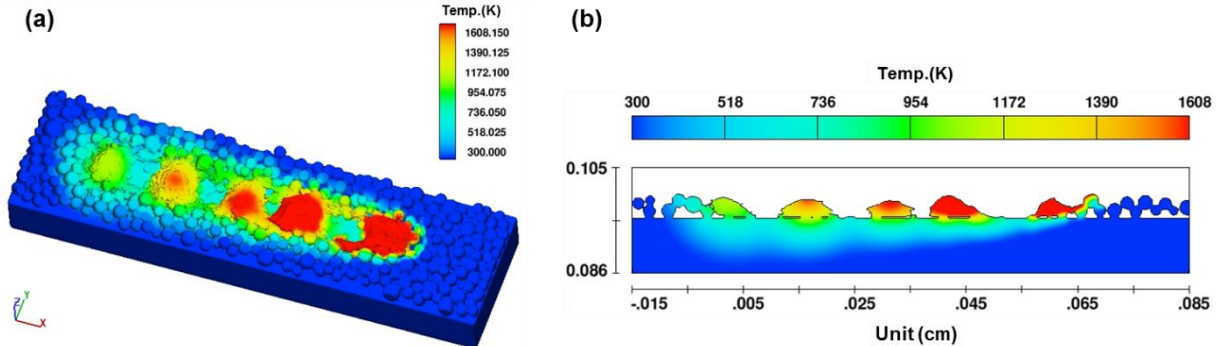


Figure 7: (a) 3D view and (b) 2D longitudinal section view of molten pool for the fast scanning speed at 2.3 m/s. All other conditions, i.e., laser power = 200W, powder packing density = 38%, and PSD+, are the same as those in Fig. 6(a).

A mechanism for forming the disconnected balls in high speed laser melting is attributed to the Rayleigh instability [14]. In particular, it states that the instability is initiated when the length to width ratio of the molten pool is greater than π . As the laser scanning speed increases, the molten pool length increases while the pool width would decrease slightly. Hence, the length to width ratio increases with faster scanning speed, which leads to a larger instability. Other factors for formation of balling defect in L-PBF include the local powder particle arrangement, wetting, Marangoni flow and gravity [5].

To further understand the formation of balling defect in L-PBF, the transient evolution of molten pool profile is illustrated in Fig. 8. As shown in this series of images, the primary molten

pool directly underneath the laser beam is not stable and the rear end quickly breaks apart from the front to form a separate island. It is interesting to observe that the separation initiates from a void in the middle of the molten pool, as shown in Fig. 8(c). This void expands as the laser continues to travel forward, eventually breaking the molten pool into two parts, as shown in Fig. 8(e) and 8(f). The formation of void and its expansion are likely caused by the strong backward flow driven by the surface tension described previously. The length to width ratio for the molten pool shown in Fig. 8 is approximately 2.3, which is lower than the threshold ratio for Rayleigh instability. This indicates that the relatively low packing density (when compared to a solid) could increase the likeliness of forming the balling defect.

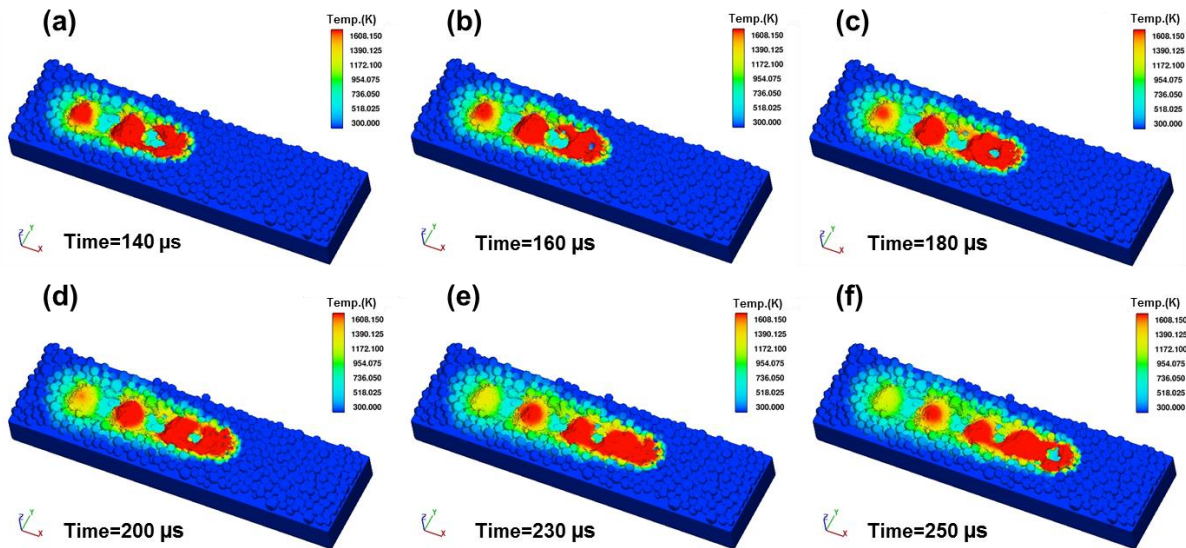


Figure 8: Evolution of molten pool profile illustrating the formation of balling defect.

3.3.3. Effect of laser power

From the perspective of heat input per unit length, a faster travel speed is equivalent to a lower laser power. To examine the effect of lowering the laser power on the formation of balling defect, a laser power of 150W is considered while all other conditions are kept the same as those in Fig. 6(a). As shown in Fig. 9, a reduction in the laser power indeed results in a discontinuous molten pool and the formation of balling defect. On the contrary, a higher laser power is desirable to minimize the balling defect when faster travel speed is used. However, the literature data has shown an overly high laser power can worsen the surface finish [13]. The effect of high laser power on surface roughness will be the subject of a future study.

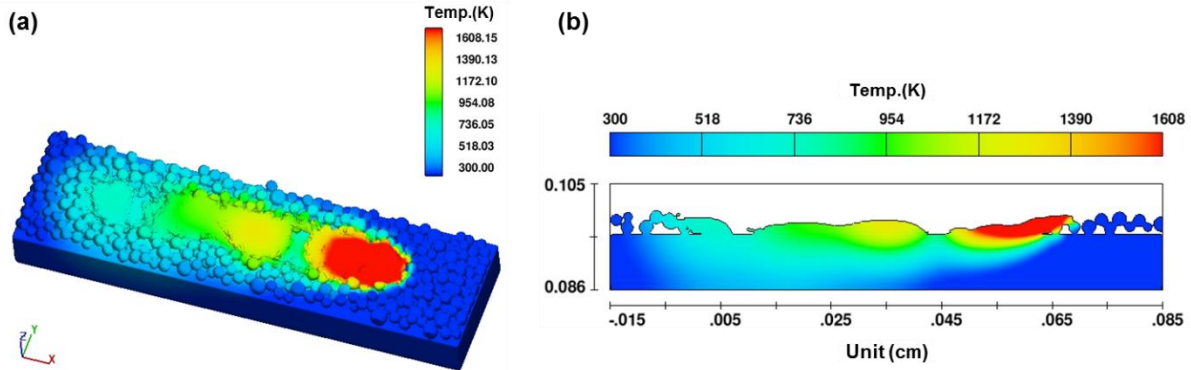


Figure 9: (a) 3D view and (b) 2D longitudinal section view of molten pool for the low laser power of 150 W. All other conditions, i.e., scanning speed = 1.1 m/s, powder packing density = 38%, and PSD+, are the same as those in Fig. 6(a).

3.3.4. Effect of packing density

The last factor to be examined is the powder packing density. Literature data has shown that a higher powder packing density is desirable to produce dense parts with better surface finish [1,15]. Figure 10 shows the molten pool profile for a packing density of 45%. All other parameters are the same as those in Fig. 9. As shown in Fig. 10, an increase in packing density from 38% to 45% eliminates the discontinuous molten pool and produces a smoother surface contour. As discussed previously, the balling defect initiates from a void at the center of the molten pool (see Fig. 8). Higher packing density is expected to reduce the formation of such void due to a larger mass to fill any new void. In addition, it is reported that a relatively lower packing density enhances fluid convection especially in the downward direction driven by gravity due to higher porosity [16]. Such strong downward fluid convection can further increase the instability of the molten pool, resulting in formation of balling defect.

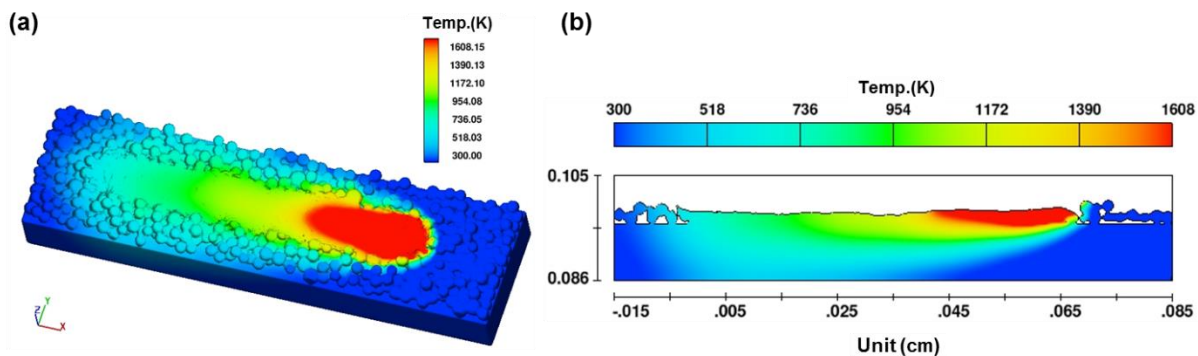


Figure 10: (a) 3D view and (b) 2D longitudinal section view of molten pool for the high powder packing density of 45%. All other conditions, i.e., laser power = 150 W, scanning speed = 1.1 m/s, and PSD+, are the same as those in Fig. 9.

4. Summary and conclusion

In summary, the 3D transient simulation of heat transfer and fluid flow in L-PBF is conducted to provide a quantitative understanding of the effect of key processing parameters on bead geometry and formation of balling defect. The 3D model solves the continuum conservation equations at the meso-scale level with a mesh size of 3 μm to accurately resolve individual powder particles. The initial powder stack-up is calculated using a DEM based model and inputted into the 3D model. Through the numerical investigation of a variety of processing variables, the following conclusions can be drawn:

- A positively skewed particle size distribution containing a high fraction of smaller particles results in a smoother contour of the melt pool than the negatively skewed one containing a high fraction of larger particles.
- The formation of balling defect initiates from a void at the center of the molten pool. As the void expands, the molten pool breaks apart into separate islands.
- A faster travel speed and lower laser power can increase the likeliness of forming the balling defect.
- In addition to Rayleigh instability designated by the length to width ratio of the molten pool, the powder particle arrangement (i.e., the powder packing density) has a significant effect on the formation of balling defect. A higher packing density is found to reduce the likeliness of forming such defect.

Although only a simple linear track is simulated, the present model shows the importance of powder level simulation in studying the meso-scale phenomena including molten pool surface profile and formation of balling defect, which are important attributes of the final build quality.

Acknowledgements

The authors would like to acknowledge the grant from Office of Naval Research (ONR), Award No. N00014-14-1-0688, in support of the research.

References

1. Korner C, Bauereiss A, Attar E (2013) Fundamental consolidation mechanisms during selective beam melting of powders. *Model Simul Mater Sci Eng* 21(8):085011.
2. Klassen A, Bauereiss A, Korner C (2014) Modelling of electron beam absorption in complex geometries. *J Phys D-Appl Phys* 47(6):065307.
3. King W, Anderson AT, Ferencz RM, Hodge NE, Kamath C, Khairallah SA (2015) Overview of modelling and simulation of metal powder bed fusion process at Lawrence Livermore National Laboratory. *Mater Sci Technol* 31(8):957-968.
4. Matsumoto M, Shiomi M, Osakada K, Abe F (2002) Finite element analysis of single layer forming on metallic powder bed in rapid prototyping by selective laser processing. *Int J Mach Tools Manuf* 42(1):61-67.
5. Korner C, Attar E, Heintz P (2011) Mesoscopic simulation of selective beam melting processes. *J Mater Process Technol* 211(6):978-987.
6. Khairallah SA, Anderson A (2014) Mesoscopic simulation model of selective laser melting of stainless steel powder. *J Mater Process Technol* 214(11):2627-2636.

7. Gurtler FJ, Karg M, Leitz KH, Schmidt M (2013) Simulation of laser beam melting of steel powders using the three-dimensional volume of fluid method. *Phys Proced* 41:874-879.
8. Šmilauer V, Catalano E, Chareyre B, Dorofeenko S, Duriez J, Gladky A, Kozicki J, Modenese C, Scholtès L, Sibille L, Stránský J, and Thoeni K (2010) Yade documentation (šmilauer v, ed.), The Yade project, 1st ed., <http://yade-dem.Org/doc/>
9. Flow3d: Version 11.0.1.2 (2014): User manual, Flowscience, Santa Fe, NM, USA.
10. Cho MH, Lim YC, Farson DF (2006) Simulation of weld pool dynamics in the stationary pulsed gas metal arc welding process and final weld shape. *Weld J* 85(12):271S-283S.
11. Boley CD, Khairallah SA, Rubenchik AM (2015) Calculation of laser absorption by metal powders in additive manufacturing. *Appl Optics* 54(9):2477-2482.
12. Spierings A, Levy G (2009) Comparison of density of stainless steel 316L parts produced with selective laser melting using different powder grades. In *Proc of the Annual Int Solid Freeform Fabrication Symp.* University of Texas at Austin, Austin, pp 342-353
13. Liu B, Wildman R, Tuck C, Ashcroft I, Hague R (2011) Investigation the effect of particle size distribution on processing parameters optimisation in selective laser melting process. In *Proc of the Annual Int Solid Freeform Fabrication Symp.* University of Texas at Austin, Austin. pp 227-238
14. Kruth JP, Levy G, Klocke F, Childs THC (2007) Consolidation phenomena in laser and powder-bed based layered manufacturing. *CIRP Ann-Manuf Technol* 56(2):730-759.
15. Spierings A, Herres N, Levy G (2011) Influence of the particle size distribution on surface quality and mechanical properties in am steel parts. *Rapid Prototyping J* 17(3):195-202.
16. Attar E (2011) Simulation of selective electron beam melting processes. PhD thesis, University of Erlangen-Nuremberg, Erlangen, Germany